2026 IEEE International Conference on Robotics and Automation (ICRA 2026)
June 1-5, 2026. Vienna, Austria

CableSense: MuJoCo Simulation-Guided Neural Networks for Force Estimation in Cable-Driven Manipulators

Chunru Yang, Xinruo Xu, Zhongrui Cui, Yanan Li, Xueqian Wang

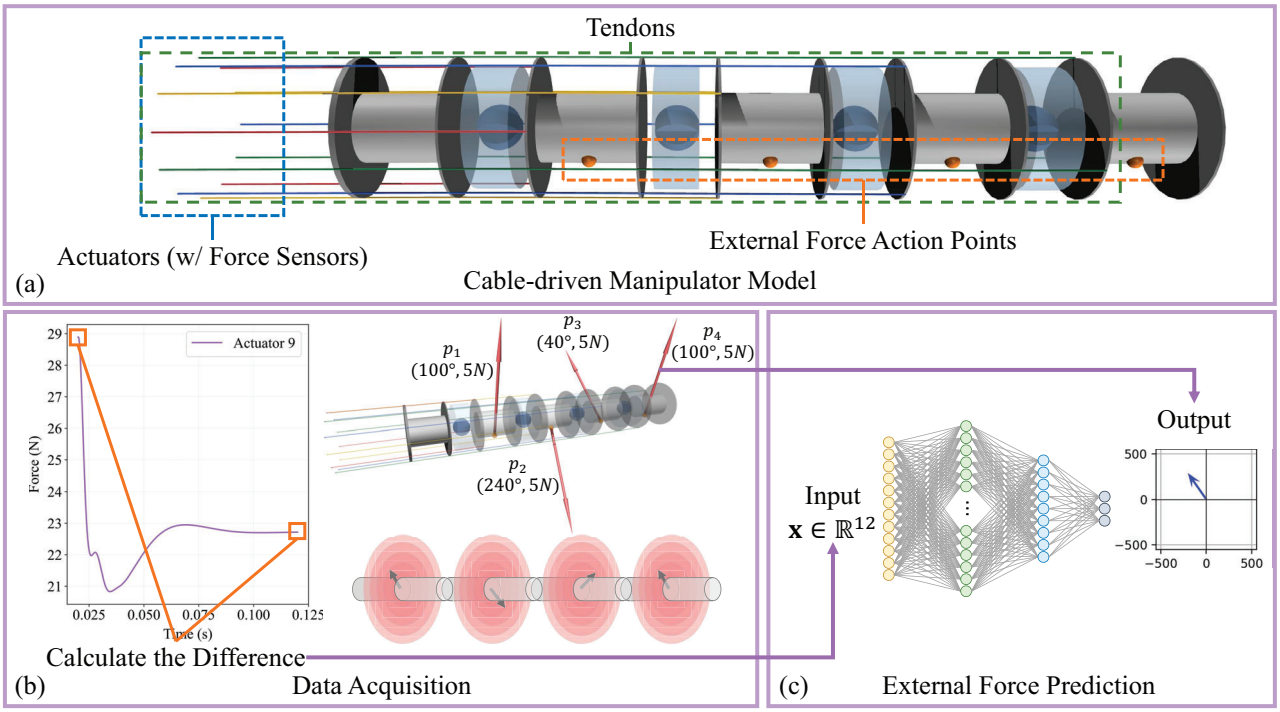

Fig. 1. Overview of CableSense. (a) Simulation model of the manipulator. Actuators are placed at the tendon ends with integrated force sensors. The four orange spheres mark external force points. (b) Data collection process. External forces (0–200N) are applied normal to the arm plane during steady state. Cable tension differences between perturbed and initial states are recorded. (c) Force perception network uses 12D cable tension inputs to estimate external force.

***Abstract*— Cable-driven serial manipulator (CDSM) has advantages of lightweight structure, high flexibility, and inherent safety, making it suitable for operations in constrained spaces. However, interaction with the environment is inevitable. To address this limitation, we propose CableSense, a novel force-sensing approach that leverages actuation cable tension information exclusively, thereby eliminating the requirement for additional contact sensors. We first develop a high-fidelity MuJoCo simulation model based on the physical system, reducing the sim-to-real gap through careful calibration of physical and mechanical parameters. Leveraging this simulation model, we generate a comprehensive dataset encompassing diverse external force scenarios. We then implement a multi-task deep learning framework CableSense, for both single-point and multi-point force identification. Experiments demonstrate that CableSense achieves over 98% accuracy in contact location estimation, maintaining a mean absolute direction error of 5.96°.**

This work was supported in part by the National Natural Science Foundation of China under Grant 52405028, in part by the National Key R&D Program of China (2022YFB4701400/4701402), in part by the China Postdoctoral Science Foundation under Grant Number 2024M761635. (Corresponding authors: Yanan Li; Xueqian Wang).

Chunru Yang, Xinruo Xu, Zhongrui Cui, Yanan Li and Xueqian Wang are with Shenzhen International Graduate School, Tsinghua University, Shenzhen 518055, China. (e-mail: ycr24@mails.tsinghua.edu.cn; xuxr24@mails.tsinghua.edu.cn; cuizr24@mails.tsinghua.edu.cn; yananli@sz.tsinghua.edu.cn; wang.xq@sz.tsinghua.edu.cn).

I. INTRODUCTION

Compared with rigid actuation, cable transmission not only reduces the payload at the end-effector but also enhances safety during physical interactions with the environment. Therefore, it has broad applications in soft hand [1]–[3], tensegrity robot [4], [5]. However, achieving safe and stable interaction in complex environments requires accurate external force perception. Traditional approaches often rely on force/torque sensors mounted at the end-effector or joints, but such sensors are costly and difficult to integrate within a slender body. Cable-driven manipulators, by design, maintain intrinsic compliance and low impedance; their bodies typically lack extensive rigid shells, making it difficult to integrate dense tactile or contact force sensor arrays on their surfaces. Simultaneously, the wiring of external sensors significantly increases system mass and mechanical impedance, further compromising motion performance [14], [15].

TABLE I. Overview of application of tendon in MuJoCo

Literature	Robot Type	Physical/Simulation	Position/Force Control
[6], [7]	Tendon-driven manipulator	Simulation	Position Control
[3]	Soft wearable robot	Physical	Force Control
[8]	Tendon-driven robotic limb	Simulation	Position and Force Control
[9]	Tendon-driven quadruped robot	Simulation	Position and Force Control
[10]	Tendon-driven anthropomorphic hand	Simulation	Position Control
[11]	Tendon-driven continuum robot	Simulation	Position and Force Control
[12]	Musculoskeletal simulation	Simulation	Model Predictive Control
[4], [5]	Tensegrity robot	Simulation	Force Control
[13]	Musculoskeletal-Exoskeletal Hybrid	Simulation	Position Control
[1]	Tendon-driven Robotic Hand	Physical	Position Control
[2]	Tendon-driven finger	Simulation	Force Control

To overcome these limitations, some researchers have proposed model-based external force estimation methods, in which system dynamics models and state observers are employed to infer external forces. Rucker et al. [16], [17] established a static and dynamic consistent model coupling Cosserat-rod and Cosserat-string theories, laying the theoretical groundwork for identifying external loads and their application points within a continuum framework. Building on this, Back et al. [18] utilized a real-time Cosserat model and shape observation to achieve online estimation of catheter contact forces without external tactile sensing. Additionally, some rapid methods, such as those using local curvature characterization with least-squares solvers, can significantly reduce computation time [19].

However, for cable-driven robots with multiple points of contact, these methods are computationally inefficient and rely on high-precision system modeling, limiting their practical application. First, the computational burden of boundary value or constrained problems increases significantly with the number of degrees of freedom or contact points [20]. Second, their accuracy is susceptible to degradation from non-ideal factors like tendon-backbone friction, backlash, and hysteresis [21], [22]. Third, these models are often tailored for specific mechanisms and boundary conditions, limiting their cross-platform generalizability and parameter portability [23], [24].

Neural networks have been increasingly adopted for force perception in robotic manipulators due to their powerful nonlinear approximation capability. Shan et al. [25] proposed a neural network–based approach that optimizes the training data structure to achieve real-time external force estimation without external force/torque sensors; Wu et al. [26] combined convolutional neural networks with gated recurrent units to estimate contact forces in heavy-duty robots using actuation signals and motion information. Lim et al. [27] introduced MOB-Net, which integrates internal inertial measurement units and joint encoder signals to perform online estimation of external joint torques in humanoid robots. These methods leverage actuation signals and dynamic observations to circumvent complex sensor deployment while preserving the inherent compliance.

While existing studies have demonstrated promising results for rigid manipulators, their application to cable-driven robots remains challenging. On the one hand, the complex characteristics of rope transmission, such as nonlinearity, friction, and relaxation, are difficult to capture directly through simplified models. On the other hand, existing simulation-based training often lacks physical properties consistent with the real system, making it difficult to transfer the perception model to the actual robot system. As shown in Table I, the majority of studies [8]–[13] that model cable using MuJoCo are conducted solely in simulation and lack validation with physical hardware.

We propose a comprehensive solution that combines simulation and data-driven learning. The research pipeline is illustrated in Fig. 1. We first developed a high-fidelity model of CDSM in MuJoCo. The mechanical parameters of this model (e.g., dimensions, mass, stiffness, damping) are meticulously configured to match the physical platform, ensuring a high degree of physical realism. This model enables the efficient and controlled generation of large volumes of noise-free ”cable-tension-to-external-force” paired data.

Leveraging the vast amount of simulation data, we train an end-to-end neural network to learn the complex, nonlinear mapping from changes in cable tensions to external force information. A significant advantage of this method is that its performance is not directly affected by the mechanical complexity of the arm and it possesses strong generalization capabilities. To validate the fidelity of the simulation, we compared simulation data with data collected from physical experiments. The results demonstrate consistent trends and magnitudes between the two. Ultimately, our algorithm achieved an extremely high accuracy in simulation tests and demonstrated promising force sensing performance in preliminary physical experiments, validating the feasibility of the “simulation-to-reality” transfer.

The main contributions of this paper are summarised as follows:

1) A high-fidelity MuJoCo simulation model of a CDSM was developed, serving as a data foundation for training neural networks.
2) A systematic investigation was conducted on tendon-related properties in MuJoCo, including stiffness, friction, and actuation methods.
3) An end-to-end neural network framework was proposed for indirect force sensing relying exclusively on cable tension information, achieving over 98% accuracy in contact point prediction.

II. HIGH-FIDELITY SIMULATION FRAMEWORK

Cable-driven mechanisms enable long-distance transmission of force and displacement, offering advantages such as electromechanical separation and strong adaptability. As shown in Fig. 2, a common cable-driven transmission converts the rotational motion of a motor into linear motion via a ball screw, thereby pulling the cable.

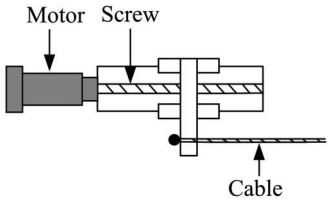

Fig. 2. Schematic diagram of cable drive mode.

The tendon should be modeled to meet the following characteristics:

- **Displacement Input**: Cable-driven robots are typically controlled by multiple cables working in coordination. Since the input control force cannot be directly measured, position-based actuation is generally employed instead of force-based actuation.
- **Pretension**: Pretension should be applied initially to prevent cable slack.
- **Elastic Deformation**: The relationship between cable deformation and cable tension when pulling the cable. The simplest case is a linear relationship:

$$T = \frac{EA}{L_0}(L - L_0) \tag{1}$$

  where T denotes the cable tension, E is the elastic modulus, A is the cross-sectional area, L_0 is the initial length, and L is the current length.
- **Self-locking**: The combination of a motor and a ball screw provides a self-locking function.
- **Friction**: When a cable wraps around a pulley, the tension at both ends is governed by the Capstan equation. Under sliding conditions, the output tension T_{out} and input tension T_{in} satisfy the exponential relation:

$$T_{\text{out}} = T_{\text{in}} \cdot e^{-\mu\theta} \tag{2}$$

  where μ is the friction coefficient and θ is the total wrap angle.

In MuJoCo, spatial tendons are defined as the shortest path that passes through a sequence of specified sites (or via-points) or wraps around specified geoms. To investigate different physical properties of cables, we design three tendon configurations in MuJoCo. Fig. 3(a) depicts a cable fixed at one end and driven at the other, representing the simplest model used to study intrinsic cable properties such as stiffness and pretension. Fig. 3(b) shows a cable driven at both ends, which better resembles the usage state in a manipulator and is employed to examine the self-locking characteristics of the drive system. Fig. 3(c) illustrates a cable wrapping around a cylinder, introducing contact between the cable and an object to analyze friction effects. All three cables have a length of 1 m.

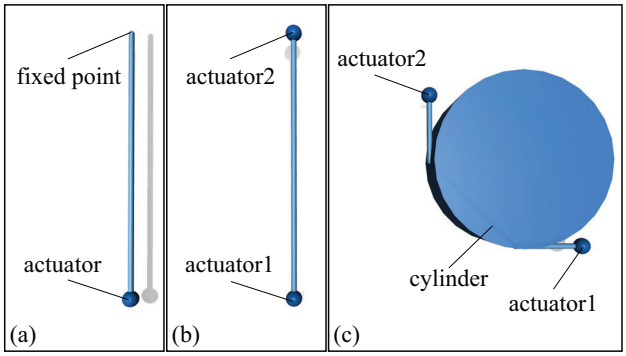

Fig. 3. Three MuJoCo tendon configurations for investigating cable properties.

A. Displacement Actuation

Cable-driven robots typically employ multi-cable coordinated control, making it difficult to directly control the input force. Therefore, a position-driven strategy is generally adopted, where the theoretical cable length is computed from joint angles and used as the control input. The displacement drive signal is shown in Fig. 4(a).

B. Pretension

To prevent cable slack, a pretension force is typically applied. This can be implemented in two ways: adding a bias to the actuator signal, or setting the springlength parameter of the tendon to enforce an initial length slightly shorter than its ideal value (i.e., the shortest path between all via points). Fig. 4(b) shows the variation in cable tension during actuation, using the tendon model illustrated in Fig. 3(a). In this model, the distance between two via points is 1 m, and the springlength is set to 0.999995 m. The initial cable tension is observed to be $50,\text{N}$, which corresponds to the applied pretension force. Note that in both Fig. 4(b) and (c), a vertical line appears at the starting point (t=0 in (b) and zero actuator position in (c)), representing a transient tension oscillation (from 0 to approximately 100 N) caused by the sudden tensioning of the cable upon simulation initialization; this oscillation quickly dampens out due to the simplicity of the model.

C. Cable Elastic Deformation

In MuJoCo, the spring deformation of tendons is defined by the stiffness parameter. The stiffness is typically calculated using the following formula:

$$k = \frac{EA}{L_0} \tag{3}$$

Based on the physical system, we set this value to $10^7 N/m$. Fig. 4(c) illustrates the variation in cable tension during the actuation process. The results clearly show that the cable tension remains proportional to the cable deformation, with the proportionality constant equal to the stiffness value.

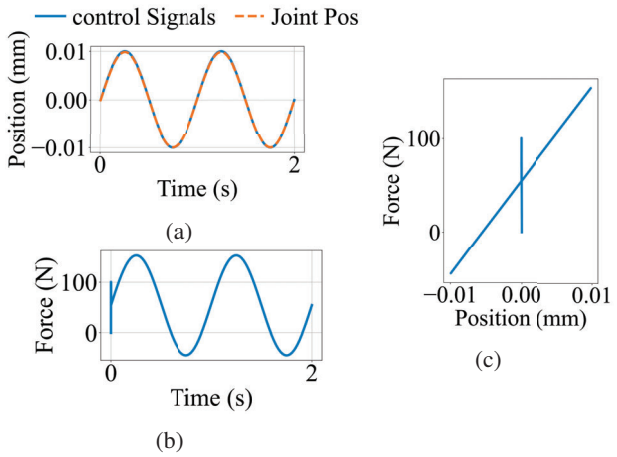

Fig. 4. MuJoCo simulation results. (a) Actuator position over time (drive signal). (b) Cable tension over time, showing a proportional relationship with actuator position. (c) Cable tension versus actuator position. Since the initial actuator position is zero, actuator position numerically equals cable deformation, directly illustrating the proportional relationship between tension and deformation.

D. Self-locking

Real-world systems often use a "motor + ball screw" configuration to achieve self-locking. Although MuJoCo provides a position actuator, self-locking is difficult to achieve due to joint coupling, manifested as the joint failing to reach the target position accurately (Fig. 5), using the tendon model illustrated in Fig. 3(b). The underlying reason is that the actuator torque is insufficient to resist the high tension generated by cable deformation. Experiments show that setting the proportional gain k_p approximately one order of magnitude higher than the stiffness value effectively alleviates this issue. Although a small steady-state error remains, excessively high k_p can cause numerical instability. Therefore, we use an implicit integrator and reduce the simulation timestep to improve numerical stability.

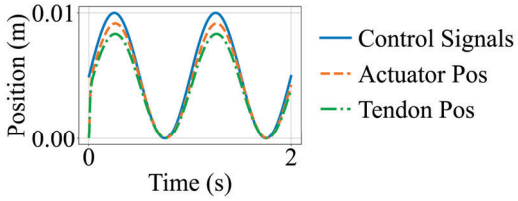

Fig. 5. Actuator position vs joint position with smaller k_p.

E. Frictional Contact

The cable passes through a series of contact points along the transmission path, where friction introduces nonlinear effects such as hysteresis. MuJoCo employs a complementarity-free method based on convex optimization and regularization to approximate friction handling.

In MuJoCo, the friction coefficient can be set via the frictionloss parameter to simulate hysteresis effects, as shown in Fig. 6.

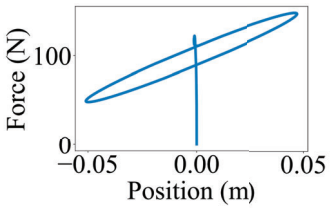

Fig. 6. Hysteresis effect caused by friction.

III. FORCE SENSING ALGORITHM

We aim to sense external forces with minimal sensors. Cable tension is ideal. Tension sensors are typically placed at cable ends (connecting ball screws and motors). A key feature of cable-driven manipulators is that the actuators (motors) are located remotely from the arm links, with motion transmitted via cables. Consequently, tension sensors can be placed at the actuator end without adding any mass or altering the structure of the moving links, thus avoiding interference with the manipulator's motion. Therefore, we propose a method using only cable tension to indirectly perceive external forces. We first build a MuJoCo model of a four-section cable-driven arm, tune parameters to match the physical system, and then collect 5000 simulated samples (single/multi-point forces) for constructing force identification networks.

A. Data Collection

The simulation model (Fig. 1(a)) is built strictly according to the physical robot (Fig. 8). As shown in the figure, the manipulator consists of four segments, each driven by three cables. The joints are cross-axis joints with two degrees of freedom.

We aim to estimate external forces using only cable tension data, thereby capturing physical interactions. Forces are assumed to be applied at the center of each segment (modeled as spheres at the bottom of the links). We consider forces in all directions normal to the arm axis (360° coverage per segment). The input features consist of tension readings from all twelve cables.

For single-point contacts, we exhaustively sample force conditions to ensure complete coverage. For multi-contact scenarios, we generate a fixed set of randomized force configurations. Each training sample includes the difference in cable tensions between perturbed and steady states, and is labeled with the contact location, direction, and force magnitude.

We visualize the force application to verify physical plausibility. Note that forces applied via MuJoCo's perturbation interface are reset after each synchronization. Therefore, to maintain consistent force visualization, the force must be re-applied at every simulation step following the step function.

B. Data Preprocessing and Loss Function Definitions

To enhance training stability and overall model performance, we conducted systematic data preprocessing and designed task-specific loss functions.

Let the ground-truth contact point labels be represented as $\mathbf{y}_{\text{body}} \in \{0,1\}^K$ (one-hot vectors, $K=4$), and the model outputs as logits vectors $\mathbf{z} \in \mathbb{R}^K$. The classification loss employs cross-entropy:

$$\mathscr{L}_{\text{body}} = -\sum_{i=1}^{K} y_{\text{body},i} \log\left(\frac{\exp(z_i)}{\sum_{j=1}^{K}\exp(z_j)}\right) \tag{4}$$

To address the discontinuity issue in angular periodicity, we map the angle $\theta \in [0^\circ, 360^\circ)$ to a two-dimensional continuous vector:

$$\mathbf{y}_{\text{angle}} = \begin{bmatrix} \sin\left(\frac{\pi\theta}{180}\right) \\ \cos\left(\frac{\pi\theta}{180}\right) \end{bmatrix}, \quad \hat{\mathbf{y}}_{\text{angle}} = \begin{bmatrix} \hat{y}_{\sin} \\ \hat{y}_{\cos} \end{bmatrix} \tag{5}$$

We utilize mean squared error (MSE) as the loss function:

$$\mathscr{L}_{\text{angle}} = \frac{1}{N}\sum_{i=1}^{N} \left\| \mathbf{y}_{\text{angle}}^{(i)} - \hat{\mathbf{y}}_{\text{angle}}^{(i)} \right\|_2^2 \tag{6}$$

Both force magnitude labels F and input features $\mathbf{x}$ undergo standardization. We employ L1 loss for supervision due to its robustness to outliers:

$$\mathscr{L}_{\text{force}} = \frac{1}{N}\sum_{i=1}^{N} \left| \tilde{F}^{(i)} - \hat{\tilde{F}}^{(i)} \right| \tag{7}$$

The overall objective function for the multi-task learning framework is then formally expressed as:

$$\mathscr{L}_{\text{total}} = \alpha \cdot \mathscr{L}_{\text{body}} + \beta \cdot \mathscr{L}_{\text{angle}} + \gamma \cdot \mathscr{L}_{\text{force}} \tag{8}$$

The selection of weighting coefficients α, β, γ is motivated by the following considerations:

- Force magnitudes exhibit a wide numerical range (0–200 N), and their unnormalized losses would dominate the overall gradient;
- After standardization, the three loss components reside in comparable numerical ranges, enabling effective balancing through weighted summation;
- L1 loss demonstrates superior robustness to outliers compared to MSE, making it suitable for force prediction scenarios where anomalous values may occur.

C. Network Architecture for Contact Force Sensing

As mentioned above, the force sensing task comprises three objectives: contact point identification, force magnitude estimation, and direction prediction.

For single-point external force identification, we first build a baseline architecture with three separate neural networks to handle each subtask independently, thus fully decoupling the tasks. This design does not account for potential inter-task correlations but aims to quickly verify the feasibility of force sensing and explore the minimal network depth and parameter count required to achieve target performance.

To further investigate interactions between tasks, we observe that contact point identification achieves the highest accuracy among the three subtasks. This is partly because it is a classification problem, which is relatively straightforward, and also because of the physical force transmission mechanism: an external force acting on a given link is transmitted backward through the preceding links and ultimately to the cables connected to those links. Consequently, the contact point location directly determines how many cables are affected—the closer the contact point is to the distal end, the more cables are influenced, making contact point recognition inherently more reliable. Therefore, we design a two-stage architecture, as seen in Fig. 7, which first identifies the contact point and then concatenates its one-hot encoded output with the raw input features $\mathbf{x}$ to serve as the input to the second stage, which jointly regresses force magnitude and direction. This design explicitly uses contact information to guide force and direction regression, aligning well with physical intuition.

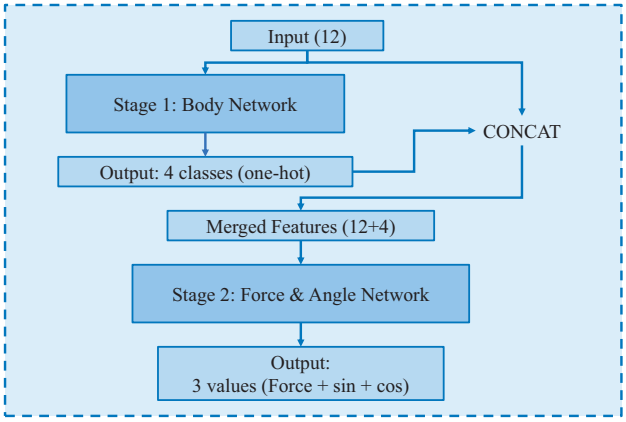

Fig. 7. Pipeline of our two-stage network.

The mathematical formulation of the two-stage fusion architecture is as follows:

First stage (contact point recognition):

$$\mathbf{p} = \text{softmax}(f_{\text{body}}(\mathbf{x})) \tag{9}$$

$$\mathbf{c} = \text{one-hot}(\arg\max(\mathbf{p})) \tag{10}$$

Second stage (force and direction regression):

$$\mathbf{h} = \phi([\mathbf{x};\mathbf{c}]) \tag{11}$$

$$\hat{F} = \mathbf{w}_F^\top \mathbf{h} + b_F \tag{12}$$

$$[\hat{y}_{\sin}, \hat{y}_{\cos}] = \mathbf{W}_\theta \mathbf{h} + \mathbf{b}_\theta \tag{13}$$

where $\phi(\cdot)$ represents the shared feature extraction layers, $[\cdot;\cdot]$ denotes vector concatenation, and $\mathbf{W}_\theta \in \mathbb{R}^{2\times d}$ is the weight matrix for angle prediction.

For multi-point force identification, we focus on pressure distribution during wrapping grasps, primarily concerning contact points and force magnitudes to avoid excessive

local pressure. Since the robotic arm maintains a relatively fixed joint configuration during wrapping, angle prediction is less relevant and thus omitted. We adopt a two-stage architecture similar to that of the single-point task, still using 12-dimensional tension differences as input. The first stage identifies contact points, and the second estimates force magnitude. The model is optimized using adaptive momentum optimization with a learning rate reduction scheduler for dynamic learning rate adjustment. And we incorporate the F1-score into the evaluation of contact point recognition to better assess positive class performance:

$$\mathrm{F1}_{\mathrm{macro}} = \frac{1}{M}\sum_{i=1}^{M}\frac{2\cdot \mathrm{precision}_i \cdot \mathrm{recall}_i}{\mathrm{precision}_i + \mathrm{recall}_i} \tag{14}$$

The learning rate scheduling strategy is:

$$\eta_{t+1} = \eta_t \cdot \lambda \cdot \mathbb{I}(\mathscr{L}_t > \mathscr{L}_{t-\Delta} \cdot (1-\varepsilon)) \tag{15}$$

where λ is the decay factor, ε is the tolerance threshold, and $\mathbb{I}(\cdot)$ is the indicator function.

IV. EXPERIMENTS

The chapter systematically validates the reliability of the simulation model through experiments and evaluates the performance of various force identification algorithms across different tasks. The physical platform of CDSM is shown in Fig. 8 [28].

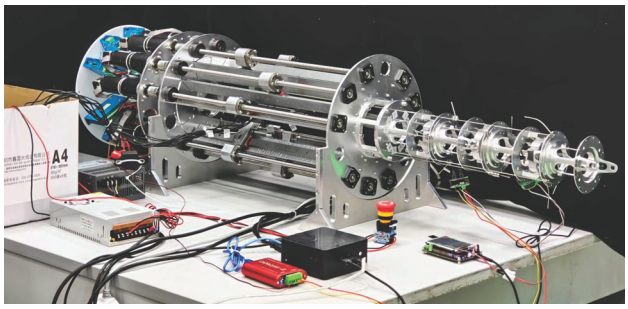

Fig. 8. The physical platform of CDSM.

A. Simulation Model Validation

High-fidelity simulation models form the basis for subsequent algorithm development. We first validate the model's kinematic behavior and sensor outputs.

A periodic oscillatory trajectory with joint angles set to $[-10^\circ, 0^\circ, 10^\circ, 0^\circ]$ is applied to the arm within a plane. As shown in Fig. 9, the joint angles accurately track the reference (left subplot of Fig. 9a), while all cable tensions fluctuate slightly around the pre-tension level (right subplot), indicating kinematically consistent actuation without significant internal forces. The actuator tracking errors in Fig. 9b further confirm the effectiveness of the position control strategy.

To evaluate simulation realism, physical cable tension changes under various loads are compared with simulation

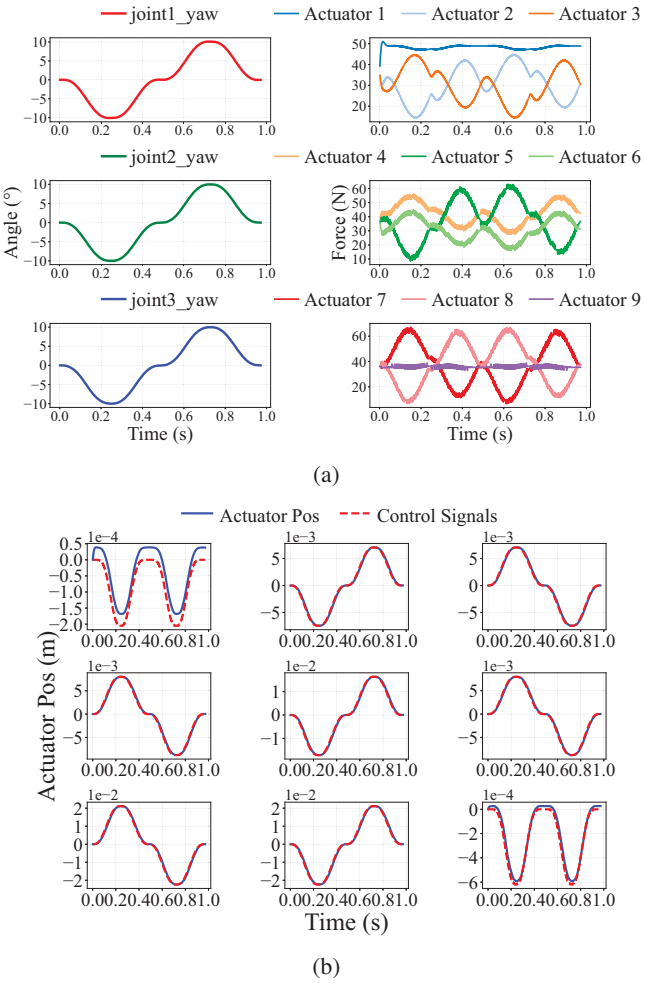

Fig. 9. Kinematic validation results. (a) Joint angles and cable tensions during kinematic validation. (b) Actuator position tracking errors during kinematic validation.

results in Table II. The trends show strong consistency, with absolute errors remaining within acceptable bounds. The maximum observed error is 5.98 N under a 2 kg load, which corresponds to approximately 30.5% of the force generated by that load (assuming standard gravity). This demonstrates that the simulation reliably replicates the mechanical characteristics of the real system, providing a credible foundation for algorithmic validation.

B. Single-Point Force Identification Task

The model's performance on single-point force identification was evaluated in simulation using comprehensive quantitative metrics and visualizations. As shown in the confusion matrix (Fig. 10), the model achieves over 98% accuracy in contact point classification, with misclassifications primarily occurring between adjacent points—especially at the distal end—and decreasing with distance from the true contact, reflecting higher sensory similarity among neighboring points.

The angle prediction errors in the simulation are tightly clustered near zero, as shown in Fig. 11, with a mean ab-

TABLE II. Comparison of simulated and measured cable tensions under different loads (N).

Condition		Cable tension								
		1	2	3	4	5	6	7	8	9
1kg Seg1	Phys	9.43	-4.53	-4.35	-0.54	-0.54	0.00	1.27	1.45	1.45
	Sim	6.66	-3.89	-3.89	-1.66	-0.38	0.90	-0.54	-0.54	-0.06
1kg Seg2	Phys	18.86	-8.52	-9.07	6.71	-0.18	-6.71	1.81	1.63	1.09
	Sim	14.93	-8.04	-8.04	5.89	-0.39	-6.67	-0.58	-0.58	-0.03
1kg Seg3	Phys	18.49	-8.52	-9.07	15.41	0.73	-14.32	4.90	4.53	-7.98
	Sim	14.84	-7.99	-7.99	13.02	-0.38	-13.78	3.77	3.77	-8.70
2kg Seg1	Phys	18.67	-8.52	-9.25	-0.91	-0.73	-0.18	2.54	2.72	2.72
	Sim	15.56	-8.36	-8.36	-1.77	-0.40	0.97	-0.56	-0.56	-0.08
2kg Seg2	Phys	38.07	-17.22	-17.95	14.87	0.18	-14.32	3.26	2.90	3.08
	Sim	32.10	-16.69	-16.69	13.29	-0.44	-14.17	-0.67	-0.67	-0.04
2kg Seg3	Phys	36.99	-17.22	-17.95	33.00	3.81	-26.83	9.43	8.88	-15.59
	Sim	31.91	-16.60	-16.60	27.56	-0.43	-28.42	8.02	8.02	-17.36

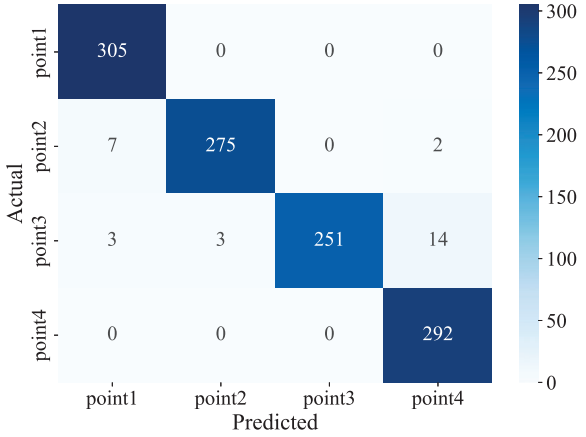

Fig. 10. Confusion matrix for the contact point classification task. The matrix shows the classification results of the model on the test set for four different contact points.

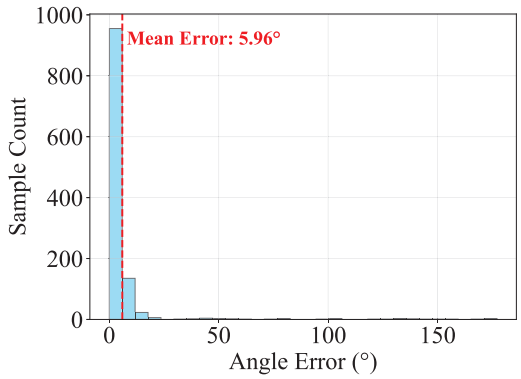

Fig. 11. Histogram of the absolute error distribution for direction prediction. The red dashed line indicates the mean absolute error of 5.96°.

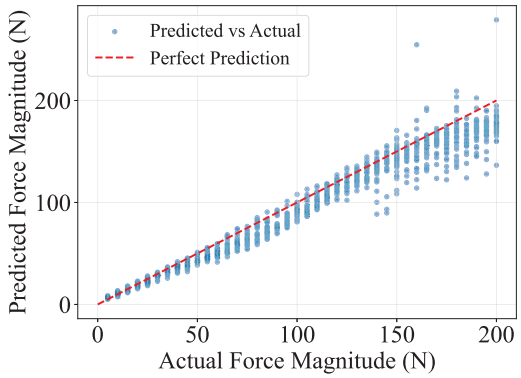

Fig. 12. Predicted vs. actual on force magnitude values.

solute error (MAE) of 5.96°. Although the error distribution exhibits some outliers, the vast majority of predictions fall within a small range. For force magnitude regression in simulation (Fig. 12), the model achieves an MAE of 9.97 N and RMSE of 14.26 N, with points closely distributed along the ideal line. Absolute error increases with force magnitude, consistent with heightened system nonlinearity and sensor uncertainty under larger loads, yet overall performance remains satisfactory.

C. Multi-Point Force Identification Task

We evaluated the multi-point force identification model in simulation using a procedure consistent with the single-point task. The model achieved over 99% accuracy in contact recognition on the simulation test set (Fig. 13), demonstrating strong classification performance. Force magnitude predictions in simulation (Fig. 14) show improved concentration and reduced error compared to the single-point case, owing to the constrained force range. Prediction errors decrease progressively from point1 to point4, consistent with the structural characteristics of the manipulator and aligned with physical expectations.

V. CONCLUSION AND FUTURE WORK

In this paper, we presented CableSense, a simulation-guided deep learning framework for external force estimation in CDSM. A high-fidelity MuJoCo model accurately captures tendon stiffness and pulley friction, enabling large-scale dataset generation for mapping cable tensions to external forces. Systematic architectural exploration shows that task-specific networks achieve high precision, while shared-backbone designs offer a favorable performance-efficiency trade-off. Our approach achieves near-perfect accuracy in contact point identification and provides reliable force direction and magnitude estimates.

Future research will focus on:

1) Incorporating temporal modeling to capture dynamic force interactions.
2) Investigating domain adaptation and transfer learning techniques to bridge the sim-to-real gap.
3) Integrating the force perception capability into closed-loop control policies for reactive and compliant manipulation.

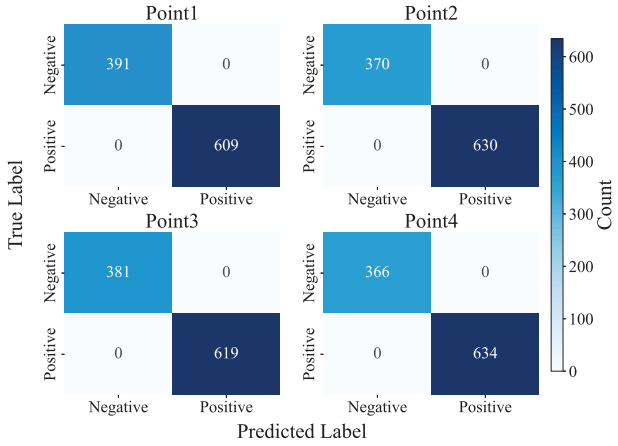

Fig. 13. Confusion matrix for contact point recognition.

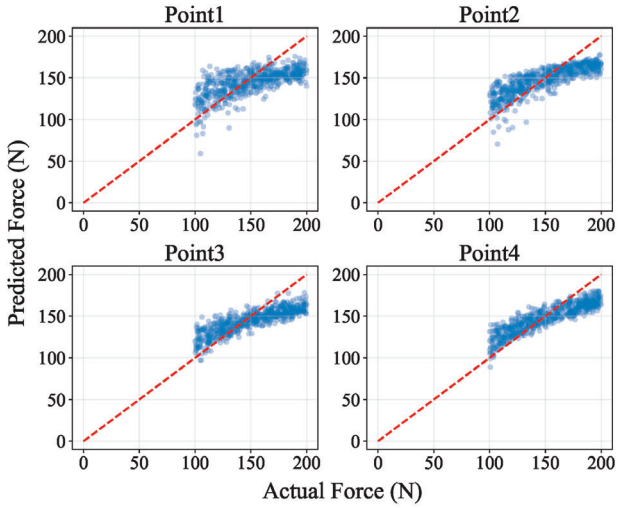

Fig. 14. Force magnitude prediction results.

REFERENCES

[1] Z. Xu, V. Kumar, and E. Todorov, "The uw hand: A low-cost, 20-dof tendon-driven hand with fast and compliant actuation," *The International Journal of Robotics Research*, p. 16, 2013.

[2] W. Zhang, B. G. Cangan, T. Buchner, A. M. Kübler, R. Asmus, and R. K. Katzschmann, "Task-defined pulley design for nonlinearly coupled tendon-driven actuation," in *2024 IEEE 7th International Conference on Soft Robotics (RoboSoft)*. IEEE, 2024, pp. 220–227.

[3] B. Kim, U. Jeong, and K.-J. Cho, "Exo-glove pinch: A soft, hand-wearable robot designed through constrained tendon routing analysis," *IEEE Robotics and Automation Letters*, 2025.

[4] R. Terajima, K. Inoue, S. Yonekura, K. Nakajima, and Y. Kuniyoshi, "Behavioral diversity generated from body–environment interactions in a simulated tensegrity robot," *IEEE Robotics and Automation Letters*, vol. 7, no. 2, pp. 1597–1604, 2021.

[5] R. Terajima, K. Inoue, K. Nakajima, and Y. Kuniyoshi, "Multifunctional physical reservoir computing in soft tensegrity robots," *Chaos: An Interdisciplinary Journal of Nonlinear Science*, vol. 35, no. 8, 2025.

[6] M. Ishige, T. Taniguchi, and Y. Kawahara, "Dream to pose in a tendon-driven manipulator with muscle synergy," in *2022 IEEE International Conference on Development and Learning (ICDL)*. IEEE, 2022, pp. 250–256.

[7] K. Or, K. Wu, K. Nakano, M. Ikeda, M. Ando, Y. Kuniyoshi, and R. Niiyama, "Curriculum-reinforcement learning on simulation platform of tendon-driven high-degree of freedom underactuated manipulator," *Frontiers in Robotics and AI*, vol. 10, p. 1066518, 2023.

[8] A. Marjaninejad, J. Tan, and F. Valero-Cuevas, "Autonomous control of a tendon-driven robotic limb with elastic elements reveals that added elasticity can enhance learning," in *2020 42nd Annual International Conference of the IEEE Engineering in Medicine & Biology Society (EMBC)*. IEEE, 2020, pp. 4680–4686.

[9] A. Marjaninejad and F. J. Valero-Cuevas, "Model-agnostic bio-inspired autonomous lifelong-learning of kinematic control in tendon-driven quadruped robots," in *2024 10th IEEE RAS/EMBS International Conference for Biomedical Robotics and Biomechatronics (BioRob)*. IEEE, 2024, pp. 612–618.

[10] P. Polcz, K. Schäffer, and M. Koller, "Posture estimation for a high degree of freedom anthropomorphic tendon-based hand model–a simulation experiment," in *2024 European Control Conference (ECC)*. IEEE, 2024, pp. 591–596.

[11] P. Rao, "Tendon driven continuum robots: Modeling and motion planning for contact aided navigation and shape locking," Ph.D. dissertation, University of Toronto (Canada), 2024.

[12] Y. Sahara, A. Miki, Y. Ribayashi, S. Yoshimura, K. Kawaharazuka, K. Okada, and M. Inaba, "Construction of musculoskeletal simulation for shoulder complex with ligaments and its validation via model predictive control," in *2024 IEEE/RSJ International Conference on Intelligent Robots and Systems (IROS)*. IEEE, 2024, pp. 327–333.

[13] H. Wang, V. Caggiano, G. Durandau, M. Sartori, and V. Kumar, "Myosim: Fast and physiologically realistic mujoco models for musculoskeletal and exoskeletal studies," in *2022 International Conference on Robotics and Automation (ICRA)*. IEEE, 2022, pp. 8104–8111.

[14] C. Zhao, Z. Chen, Y. Zheng, C. Deng, Z. Liu, J. Jiang, H. Yan, and G. Zheng, "Collaborative biomimetic external analysis system combined with artificial intelligence for human augmentation," *Sensors and Actuators A: Physical*, p. 116860, 2025.

[15] S. Zhou, Y. Li, Q. Wang, and Z. Lyu, "Integrated actuation and sensing: Toward intelligent soft robots," *Cyborg and Bionic Systems*, vol. 5, p. 0105, 2024.

[16] D. C. Rucker and R. J. Webster III, "Statics and dynamics of continuum robots with general tendon routing and external loading," *IEEE Transactions on Robotics*, vol. 27, no. 6, pp. 1033–1044, 2011.

[17] D. C. Rucker, B. A. Jones, and R. J. Webster III, "A geometrically exact model for externally loaded concentric-tube continuum robots," *IEEE Transactions on Robotics*, vol. 26, no. 5, pp. 769–780, 2010.

[18] J. Back, T. Manwell, R. Karim, K. Rhode, K. Althoefer, and H. Liu, "Catheter contact force estimation from shape detection using a real-time cosserat rod model," in *2015 IEEE/RSJ International Conference on Intelligent Robots and Systems (IROS)*, 2015, pp. 2037–2042.

[19] Q. Xiao and Y. Chen, "Efficient force estimation for continuum robot," *arXiv preprint arXiv:2109.12469*, 2021.

[20] J. Till, V. Aloi, and C. Rucker, "Real-time dynamics of soft and continuum robots based on cosserat rod models," *The International Journal of Robotics Research*, vol. 38, no. 6, pp. 723–746, 2019.

[21] T. Do, T. Tjahjowidodo, M. W. S. Lau, and S. J. Phee, "A new approach of friction model for tendon-sheath actuated surgical systems: Nonlinear modelling and parameter identification," *Mechanism and Machine Theory*, vol. 85, pp. 14–24, 2015.

[22] K. Oliver-Butler, J. Till, and C. Rucker, "Continuum robot stiffness under external loads and prescribed tendon displacements," *IEEE transactions on robotics*, vol. 35, no. 2, pp. 403–419, 2019.

[23] P. Rao, Q. Peyron, S. Lilge, and J. Burgner-Kahrs, "How to model tendon-driven continuum robots and benchmark modelling performance," *Frontiers in Robotics and AI*, vol. 7, p. 630245, 2021.

[24] M. Russo, S. M. H. Sadati, X. Dong, A. Mohammad, I. D. Walker, C. Bergeles, K. Xu, and D. A. Axinte, "Continuum robots: An overview," *Advanced Intelligent Systems*, vol. 5, no. 5, p. 2200367, 2023.

[25] S. Shan and Q.-C. Pham, "Fine robotic manipulation without force/torque sensor," *IEEE Robotics and Automation Letters*, vol. 9, no. 2, pp. 1206–1213, 2023.

[26] P. Wu, H. Dong, P. Li, Y. Bao, W. Dong, and L. Sun, "A new contact force estimation method for heavy robots without force sensors by combining cnn-gru and force transformation," *Technologies*, vol. 13, no. 5, p. 192, 2025.

[27] D. Lim, M.-J. Kim, J. Cha, and J. Park, "Mob-net: Limb-modularized uncertainty torque learning of humanoids for sensorless external torque estimation," *The International Journal of Robotics Research*, vol. 44, no. 1, pp. 96–128, 2025.

[28] H. Cheng, J. Tan, Y. Li, and X. Wang, "Real-time multi-contact estimation for cable-driven serial manipulator," *IEEE Robotics and Automation Letters*, 2025.